Asynchronous UKF-based Localization of an Underwater Robotic Vehicle for Aquaculture Inspection Operations

Svetlana Potyagaylo[1], Christos C. Constantinou[1], George Georgiades[1] and Savvas G. Loizou[1]

Abstract— **This paper presents a methodology for localizing an autonomous tethered underwater robotic vehicle deployed for aquaculture inspection operations. The developed methodology is based on an Asynchronous Unscented Kalman Filer (UKF) to fuse information from onboard sensors along with a'priori knowledge about the aquaculture's geometry and the underwater robot's hydrodynamics. The performance of the proposed methodology is assessed through accuracy and consistency metrics generated from simulation benchmarks.**

I. INTRODUCTION

Underwater robotics has experienced a dramatic growing in the last years due to its potentials in different undersea applications including gathering data for oceanographic needs, pipeline and harbor inspection, and monitoring aquacultures. In the report of the European Commission [1], aquaculture is called to be the fastest growing food producing sector in the world. In addition, aquaculture facilities and tasks required for their maintenance represent a great application field for underwater robots to replace humans. In aquaculture industry, the main problem is considered to be escapes of fish from the fish net cages. According to the Norwegian report of escape incidents [2], more than 60% of escapes are caused by structural failures of fish farm equipment. The main reasons for such faults are abrasion and tearing of mooring ropes, anchor chains, or holes in the fish nets from fish biting. In order to prevent such incidents, the regular inspection of all subsystems and early detection of net holes and other types of system faults are mandatory tasks in the fish producing industry.

Currently, such operations are provided by human divers. However, this task is associated with risks of human health and lives. These risks have been increasing recently because of the tendency to push fish cage systems to far-shore sites with more severe waves and currents [3], [4]. In this case, underwater unmanned vehicles appear to be a safe and cost-efficient alternative to the human diving inspection by avoiding the health and human life risks. The current work presents portions of the systems utilized in the AQUABOT project [5] an ongoing research project aimed to develop an autonomous system for visual inspection of fish farm nets and moorings by using a tethered underwater autonomous vehicle (UAV). The GPS-denied undersea environments make the autonomous operation of underwater vehicles to be one of the most challenging problem. The effective and accurate localization and control is enabled by a fusion of data from onboard sensors and a-priory knowledge about dynamic behavior of the aquaculture. The ocean currents and flows imply additional difficulties for a robot control system making a robot to deviate away from its desired state or path.

*This work was co-funded by the European Regional Development Fund and the Republic of Cyprus through the Research Promotion Foundation under research grant ΑΕΙΦΟΡΙΑ/ΓΕΩΡΓΟ/0311(ΒΙΕ)/08

[1]S. Potyagaylo, C.C. Constantinou, G. Georgiades and S. Loizou are with Mechanical and Materials Science and Engineering Department, Cyprus University of Technology, Limassol 3041, CYPRUS `svetlana.potyagaylo, c.constantinou, savvas.loizou@cut.ac.cy`

This work is aimed at modeling a sensor suite of a ROV for different aquaculture applications along with developing algorithms for localization and state estimation of the vehicle by fusing information from different sources. The sensor suite includes an Inertial Measurement Unit (IMU), a novel combined Laser Vision System (LVS), a pressure sensor for measuring the depth of the vehicle, and a tilt-compensated compass. Such a combination of the sensor can be used in localization and navigation tasks for monitoring and inspecting aquaculture installations. The additional information sources include an optical flow concept and a'priori information of the robot's hydrodynamics and the fish-net's geometry.

Several research works have been conducted recently to model a sensor suite of underwater vehicles and to localize them in undersea GPS-denied environments. Lynen et al. [6] presented measurement models of a camera-IMU system consisting of an IMU and a spherical camera for using these models in a fusion and state estimation process. Kottas and Roumeliotis in [7] investigated the observability properties of a navigation system based on camera and IMU sensors and proposed an algorithm utilizing this analysis to improve the Extended Kalman Filter (EKF) state estimator. Bloesh et al [8] considered a measurement fusion problem from an inertial sensor and a monocular camera in form of optical flow by using an UKF to estimate a robot pose over time. Karras et al [9] proposed an online asynchronous Modified Dual UKF algorithm for state and parameter estimation of an underwater vehicle that uses fused data from an IMU and a combined camera-point lasers system.

II. SYSTEM MODELING

In this section, we present the modeling of an autonomous underwater vehicle used in this work along with its sensor suite and additional information sources. The vehicle is modeled by a nonlinear 6DOF model while the hydrodynamic and geometric parameters of the model were defined by a dynamic parameter identification procedure and by using a dedicated software as described in Subsection III-A. The models of the robot's sensors including accelerometers, gyroscopes, a tilt-compensated compass, and a novel LVS are described as well. The model of the LVS is based on

978-0-933957-43-5 ©2015 MTS

This is a DRAFT. As such it may not be cited in other works.
The citable Proceedings of the Conference will be published in
IEEE Xplore shortly after the conclusion of the conference.

a'priory known information about the aquaculture geometry model that is modelled as a function of the oceans' current velocity at the aquaculture location.

A. Vehicle Model

In this work, we consider an underwater vehicle as a 6 DOF free body that can be described by the following vectors: $\boldsymbol{\eta}_1 = [x, y, z]^T$ is the position vector, $\boldsymbol{\eta}_2 = [\phi, \theta, \psi]^T$ is the orientation (Euler angle) vector (roll, pitch and yaw angles), $\boldsymbol{\nu}_1 = [u, v, w]^T$ is the body linear velocities (surge, sway and heave), $\boldsymbol{\nu}_2 = [p, q, r]^T$ is the body angular velocities, $\mathbf{a} = [a_x, a_y, a_z]^T$ is the body accelerations. Two coordination frame are used to define the vectors. The body frame is fixed to the ROV with the origin O_B located at the center of gravity of the vehicle, the X_B axis pointing forward and lying in the symmetric plane of the vehicle, the Y_B axis pointing to the right side of the vehicle, and the Z_B axis pointing downward. The inertial frame is fixed to the aquaculture (fish net cage) that can be assumed in this case since the top of the cage is static. The origin and axes of this frame are defined as follows: the origin O_I is fixed to a middle top point of the cage, the X_I points toward the North, the Y_I axis points toward the East, and the Z_I axis points downward. The described frames and vectors are shown on Fig. 1 along with the forces and moments $\boldsymbol{\tau} = [X, Y, Z, K, M, N]^T$ acting on the vehicle.

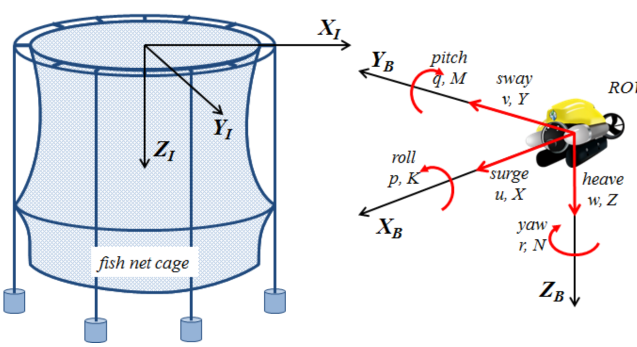

Fig. 1. Inertial and body-fixed reference frames.

We assume a full 6DOF nonlinear dynamic model of the ROV that is given by the following system of equations [10]:

$$\begin{gathered} \mathbf{M}\dot{\boldsymbol{\nu}} + \mathbf{C}(\boldsymbol{\nu})\boldsymbol{\nu} + \mathbf{D}(\boldsymbol{\nu})\boldsymbol{\nu} + \mathbf{g}(\boldsymbol{\eta}) = \boldsymbol{\tau}, \\ \dot{\boldsymbol{\eta}} = \mathbf{J}(\boldsymbol{\eta})\boldsymbol{\nu}, \end{gathered} \tag{1}$$

where $\mathbf{M}$ is the inertia matrix, $\mathbf{C}$ is the coriolis and centripetal matrix, $\mathbf{D}$ is the drag matrix, $\mathbf{g}$ is the force vector, $\boldsymbol{\tau}$ is the trust vector of forces and moments, $\boldsymbol{\nu} = \left[\boldsymbol{\nu}_1^T, \boldsymbol{\nu}_2^T\right]^T$ is the body velocities vector, $\boldsymbol{\eta} = \left[\boldsymbol{\eta}_1^T, \boldsymbol{\eta}_2^T\right]^T$ is the position and Euler angles vector, $\mathbf{J}$ is the transformation matrix from the body-fixed frame $\{B\}$ to the inertial frame $\{I\}$, where all aforementioned matrices are according to [10].

The matrices $\mathbf{M}$, $\mathbf{C}$ and $\mathbf{D}$ depend on the hydrodynamic parameters of the vehicle that represent the derivatives of the hydrodynamic forces and moments acting on the vehicle with respect to the vehicle velocities and accelerations:

$$\begin{aligned} \mathbf{M} &\sim \frac{\partial X}{\partial \dot{u}}, \frac{\partial Y}{\partial \dot{v}}, \cdots, \frac{\partial N}{\partial \dot{r}}, \\ \mathbf{C} &\sim \frac{\partial X}{\partial \dot{u}}, \frac{\partial Y}{\partial \dot{v}}, \cdots, \frac{\partial N}{\partial \dot{r}}, \\ \mathbf{D} &\sim \frac{\partial X}{\partial u}, \cdots, \frac{\partial N}{\partial r}, \frac{\partial X}{\partial u\,|u|}, \cdots, \frac{\partial N}{\partial r\,|r|}. \end{aligned} \tag{2}$$

For using the dynamic model Eq. (1) in the fusion algorithm, the model was discretized and augmented with the linear accelerations in the body frame $\mathbf{a}$. The acceleration model was derived based on the approach proposed in [9]. The final discrete model of the vehicle can be written as:

$$\begin{aligned} \boldsymbol{\nu}_{k+1} &= \boldsymbol{\nu}_k + \mathbf{M}^{-1}\left(\boldsymbol{\tau}_k - \mathbf{C}(\boldsymbol{\nu}_k)\boldsymbol{\nu}_k - \mathbf{D}(\boldsymbol{\nu}_k)\boldsymbol{\nu}_k \right. \\ &\quad \left. -\mathbf{g}(\boldsymbol{\nu}_k)\right)\Delta t, \\ \boldsymbol{\eta}_{k+1} &= \boldsymbol{\eta}_k + \mathbf{J}(\boldsymbol{\nu}_k)\boldsymbol{\eta}_k\Delta t, \\ \mathbf{a}_{k+1} &= -\mathbf{a}_k + 2\mathbf{M}^{-1}\left(\boldsymbol{\tau}_k - \mathbf{C}(\boldsymbol{\nu}_k)\boldsymbol{\nu}_k - \mathbf{D}(\boldsymbol{\nu}_k)\boldsymbol{\nu}_k \right. \\ &\quad \left. -\mathbf{g}(\boldsymbol{\nu}_k)\right). \end{aligned} \tag{3}$$

The vehicle process model we use in the localization algorithm can be written as:

$$\dot{\mathbf{x}} = f(\mathbf{x}, \mathbf{u}) + \mathbf{w}_{UAV}, \tag{4}$$

where $\mathbf{x} = \left[\boldsymbol{\nu}_1^T, \boldsymbol{\nu}_2^T, \boldsymbol{\eta}_1^T, \boldsymbol{\eta}_2^T, \mathbf{a}^T\right]^T$ is the state vector, $\mathbf{u}$ is the control (thrust) vector, $\mathbf{w}_{UAV} \sim (0, \mathbf{R}_{UAV})$ is the white noise with zero mean and the covariance matrix $\mathbf{R}_{UAV}$.

B. Sensor Models

1) Accelerometer and Gyroscope Model: We assume that the accelerometer outputs the linear accelerations $\mathbf{a}$ in the body frame, while the gyroscope measures the angular velocity $\boldsymbol{\nu}_2$ in the body frame of the ROV. These two sensors are modeled as follows:

$$\mathbf{z}_{IMU} = h_{IMU}(\mathbf{x}, \mathbf{w}_{IMU}), \tag{5}$$

where $\mathbf{w}_{IMU} \sim N(0, \mathbf{R}_{IMU})$ is the white noise with zero mean and covariance matrix $\mathbf{R}_{IMU}$.

In this equation, the vector $\mathbf{z}_g$ consists of several measurements as follows: $\mathbf{z}_{IMU} = \left[\mathbf{z}_g^T, \mathbf{z}_a^T\right]^T$, where the measurements from the gyroscope are defined as:

$$\mathbf{z}_g = [p, q, r]^T + \mathbf{w}_g, \tag{6}$$

and the measurements from the accelerometer can be written as:

$$\mathbf{z}_a = \mathbf{a} + \boldsymbol{\nu}_2 \times (\boldsymbol{\nu}_2 \times \mathbf{r}) + \boldsymbol{\alpha} \times \mathbf{r} + \mathbf{R}_{BI}^{-1}[0, 0, g]^T + \mathbf{w}_a, \tag{7}$$

where $\mathbf{R}_{BI}$ is the rotation matrix from the body to inertial frame, $\mathbf{r}$ is the position of the IMU relative to the body fixed frame, $\boldsymbol{\alpha}$ is the angular accelerations. In this expression, a compensation procedure for the "lever arm effect" is used since the accelerometer is not located at the center of mass of the UAV.

This is a DRAFT. As such it may not be cited in other works.
The citable Proceedings of the Conference will be published in
IEEE Xplore shortly after the conclusion of the conference.

2) Tilt-Compensated Compass and Depth Pressure Sensor Model: The tilt-compensated compass and the depth pressure sensor used in this work provide measurements of the current depth of the vehicle and the earth magnetic vector direction.

The depth pressure sensor is modeled based on the Pascal's Law for the hydrostatic pressure that is the force exerted on an object due to the weight of water above it:

$$\mathbf{z}_{PS} = h_{PS}\left(\mathbf{x}, \mathbf{w}_{PS}\right) = \rho g z + p_a + \mathbf{w}_{PS}, \quad (8)$$

where ρ is the water density (1000 $\mathrm{kg/m^3}$ for fresh water), g is the gravitational constant, z is the depth below the water surface, p_a is the atmosperic pressure, and $\mathbf{w}_{PS} \sim N\left(0, \mathbf{R}_{PS}\right)$ is the white noise with zero mean and covariance matrix $\mathbf{R}_{PS}$.

The tilt-compensated compass sensor provide the Euler angles of the vehicle and is modeled with the following equation:

$$\mathbf{z}_{MS} = \mathbf{V}_m + \mathbf{w}_{MS}, \quad (9)$$

where $\mathbf{V}_m = [\phi, \theta, \cos\psi, \sin\psi]$ is the Euler angles while the yaw angle is represented by its trigonometric functions to avoid the discontinuity at 0^o. $\mathbf{w}_{MS}$ is the white noise with zero mean and covariance matrix $\mathbf{R}_{PS}$.

3) Laser Vision System Model: The LVS sensor [11] consists of a CCD camera and a set of three lasers projecting the lines in the form of a triangle on the target as shown on Fig. 4. It provides the distance and orientation of a target (or aquaculture) with respect to the vehicle. In the general case, the aquaculture represents a flexible structure consisting of several parts including an array of fish net cages, mooring lines between cages and to the anchors, buoys, and weights, as it is shown on Fig. 2. In this work, we considered a fish net cage as a target for the LVS and constructed its hydrodynamic model that allows to calculate the geometry of the fish net for different environmental conditions, such as different oceans' current speeds, water density, etc. A non-linear lumped-parameters method is utilzed to model the fish net structure [12]. The net is divided into discrete quadrilateral elements (meshes) with lumped masses at the element nodes connected by massless springs. Each net element represents a structure of four interconnected bars that are subject to the external forces (hydrodynamic forces, gravity, buoyancy, inertia) applied at the center of each element. Internal (elastic) forces are incorporated into the model to address the flexibility of the net structure.

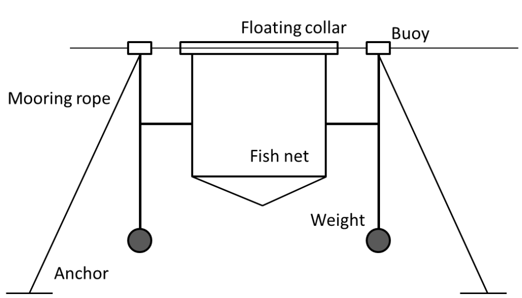

Fig. 2. Aquaculture schematic diagram.

The resulting nonlinear system of dynamic equations is solved for the 3-D coordinates of each fish net node. Note that the fish-net dynamic equations depend on the velocity of the oceans' current. This information can be acquired either by local measurements or by ocean forecasting and observation systems. In this work, we used the Cyprus Coastal Ocean Forecasting and Observing System (CYCOFOS) [13] for daily forecasting of the ocean current velocity and direction at the domain of the aquaculture. Although small modifications to the fish-net shape caused by small changes to the current velocities can be calculated on-line during the inspection task, this requires additional processing resources to be allocated to this task. To reduce the on-line computational load during sea trials an array of aquaculture geometries for several current speeds in the neighborhood of the forecasted velocities can be calculated a'priory.

The model of the fish net geometry can be considered as an additional information source and is used in the LVS measurement model as follows. The vehicle navigates around a fish cage inspecting and monitoring faults and failures of the fish net. The camera of the robot is pointing towards a target while the lasers create a triangle on the surface of the target. Since such a triangle defines a plane on the targets's surface, a relative distance and a relative orientation of the target with respect to the vehicle body frame can be calculated. The fish net geometry $\mathcal{F}$ is represented as a quad mesh with $V_{\mathcal{F}}$ vertices and $F_{\mathcal{F}}$ faces while the coordinates of the vertices are known a'priory as shown on Fig. 3. In order to compute the distance d from the vehicle position $\boldsymbol{\nu}_1 = [x, y, z]^T$ to a mesh face, we first triangulate the mesh faces by splitting each quad cell into two triangles. Then, we draw a ray $\mathbf{p}$ from the origin of the body frame along the X_B-axis of the vehicle:

$$\mathbf{p} = \mathbf{O}_B + \Delta\mathbf{p} \cdot \varepsilon, \quad \varepsilon > 0, \quad (10)$$

where $\mathbf{O}_B$ is the origin of the body frame, $\Delta\mathbf{p}$ is the X-column of the rotational matrix $\mathbf{J}_2$. The intersection point $\mathbf{P}$ of this ray with a mesh face containing vertices $\mathbf{V}_0$, $\mathbf{V}_1$ and $\mathbf{V}_2$ can be found as:

$$\mathbf{P} = \frac{-\mathbf{n} \cdot \mathbf{w}}{\mathbf{n} \cdot \Delta\mathbf{p}}, \quad (11)$$

where $\mathbf{n}$ is the normal to the current face, $\mathbf{w} = \mathbf{O}_B - \mathbf{V}_0$ is the vector between the ray origin $\mathbf{O}_B$ and the face vertex $\mathbf{V}_0$. By testing whether the intersection point is located inside the corresponding triangle face, the distance from the body frame origin to that face can be found. We proceed with the described procedure for all $2F_{\mathcal{F}}$ faces of the fish net and take the smallest distance. The orientation of the face can be calculated as a normal vector $\mathbf{n}$ to this face:

$$\mathbf{n} = \frac{\mathbf{e}_1 \times \mathbf{e}_2}{\left|\mathbf{e}_1 \times \mathbf{e}_2\right|}, \quad (12)$$

where $\mathbf{e}_1 = \mathbf{V}_0 - \mathbf{V}_1$, $\mathbf{e}_2 = \mathbf{V}_0 - \mathbf{V}_2$ are the edge vectors.

Thus, the measurement model of the LVS can be described as follows:

$$[d, \mathbf{n}]^T = h_{LVS}\left(\mathbf{x}, \mathcal{F}\right) + \mathbf{w}_{LVS}, \quad (13)$$

This is a DRAFT. As such it may not be cited in other works.
The citable Proceedings of the Conference will be published in
IEEE Xplore shortly after the conclusion of the conference.

where $\mathbf{w}_{LVS} \sim N\left(0, \mathbf{R}_{LVS}\right)$ is the zero mean white noise with covariance matrix $\mathbf{R}_{LVS}$.

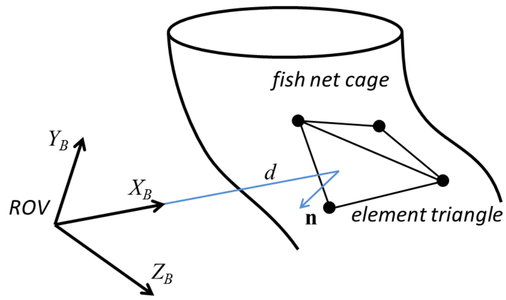

Fig. 3. The measurement model of the combined Laser Vision System.

III. System Identification and Sensor Suite Algorithms

In this section, we briefly describe the procedure implemented for identification of the vehicle parameters, particularly the hydrodynamic parameters and thrust coefficients. The algorithms used for the sensor suite operation are briefly described here as well.

A. Dynamic Parameter Identification

The vehicle used in this work is a VideoRay Pro IV ROV [14] equipped with two horizontal thrusters for surge and yaw motions and one vertical thruster for heave motion. The vehicle is under-actuated, meaning that it cannot perform sway, roll and pitch motions. The basic sensor system includes a front facing camera housed with an acrilic dome, an IMU, magnetometer and depth sensors. In addition to these sensors, the ROV was equipped with three line lasers. The combined Laser Vision System (LVS) is shown on Fig. 4. Such a set of sensors can be considered sufficient for the underwater inspection task since the IMU can provide measurements of the linear accelerations and angular rates while the LVS can calculate the relative distance and velocities with respect to the aquaculture. By incorporating the measurements from the tilt-compensated compass, the Euler angles can be estimated as well.

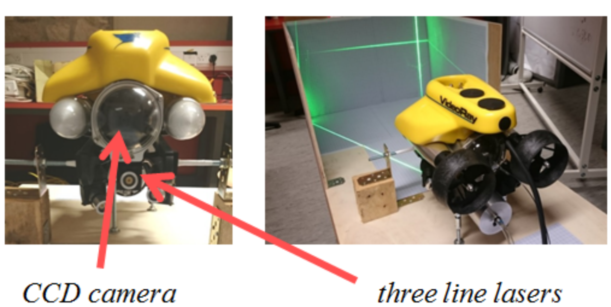

Fig. 4. A Combined Laser Vision system setup.

The accelerometer and gyroscope measurements in this work were provided by an InvenSense MPU-6050 sensor [15]. We only utilize its three-axis accelerometer and gyro providing measurements with frequency limited by a dedicated RS-485 communication line to 50 Hz. The tilt-compensated compass and the depth pressure sensor were provided with the underwater vehicle and have a working frequency of 17 Hz.

In order to identify the parameters of the underwater vehicle (e.g. entries of the matrices $\mathbf{M}$, $\mathbf{C}$, $\mathbf{D}$ and the vector $\mathbf{g}$ in the vehicle model Eq. (1)), several procedures were carried out. First, the mass and the main geometric parameters were measured while the inertia matrix of the robot about its three principal axes was calculated by using SolidWorks® software. Then, a dynamic identification procedure [16] was applied to find the hydrodynamic derivatives of the vehicles matrices Eq. (2). This procedure assumes that the vehicle model can be rewritten in a form:

$$\mathbf{Y}\boldsymbol{\pi} = \boldsymbol{\tau}, \tag{14}$$

where $\mathbf{Y}$ is the matrix of the vehicle states including velocities, accelerations, and Euler angles, $\boldsymbol{\pi}$ is the vector of unknown robot parameters including hydrodynamic derivatives and thruster coefficients, $\boldsymbol{\tau}$ is the vector of control inputs. By defining the control inputs and running experiments in a real environment, the vehicle state can be measured for each control input at each time instance.

We performed a series of experiments by exciting isolated vehicle DOFs in various frequencies. First, we forced the vehicle in the surge and yaw directions while controlling for constant depth. The second experiment was done along the surge direction while controlling for constant yaw and depth. Then, while controlling for constant yaw angle, the vehicle was exhited in the heave direction. In the next experiment the yaw direction was excited while controlling for constant depth of the robot. Finally, we performed experiments with simulatneously exciting all actuated DOFs of the vehicle (yaw, surge and heave). For each case we performed several tests by changing the amplitude and frequency of the excitation while the state of the vehicle was partially measured by its sensor suite. Measurements were then offline processed to synchronize the measurements and the control inputs and to generate the missing states (linear velocities, angular accelerations).

The described experiments were carried out in a dedicated water tank of the RCDS Lab, CUT, for about 1 min for each test. As a result, the measured states formed the matrix $\bar{\mathbf{Y}} \in \mathcal{R}^{6N\times 37}$ where N is the number of samples, the control inputs defined the vector $\bar{\tau} \in \mathcal{R}^{6N\times 1}$, while the vector of unknown parameter to be identified was of dimension $\pi \in \mathcal{R}^{37\times 1}$ for our case. The parameter vector can then be obtained as $\boldsymbol{\pi} = \bar{\mathbf{Y}}^{\dagger}\bar{\boldsymbol{\tau}}$, where $\bar{\mathbf{Y}}^{\dagger}$ is the left pseudoinverse matrix of $\bar{\mathbf{Y}}$. A more detailed description of the parameter identification procedure and results are presented in [17].

B. Laser Vision System

The CCD camera is enclosed by a hemispherical dome. Since the acrylic dome and an underwater environment affect the vision system of the ROV, a special camera calibration process was used and appropriate optic models

This is a DRAFT. As such it may not be cited in other works.
The citable Proceedings of the Conference will be published in
IEEE Xplore shortly after the conclusion of the conference.

were developed [18]. The camera has $150°$ field of view before the calibration and a resolution of 720 by 576 pixels and provides an image with the frequency of $25\,\mathrm{Hz}$. Three $532\,\mathrm{nm}$ lasers, each project a line within an $90°$ cone. Using the hemispherical optics model [18] and by knowing the laser planes, the 3D position of the laser projections are estimated [11].

IV. Asynchronous Unscented Kalman Filter Algorithm

In this work, we applied an UKF scheme to estimate the states of the vehicle. Since the measurements from the IMU, pressure and LVS sensors could arrive with different frequencies and asynchronously, the UKF algorithm was modified to incorporate this feature using the approach similar to [9], [19]. In the general case, the robot's sensor suite provides measurements with constant and high frequency, while the frequency of the LVS and optical flow is much lower and can vary depending on computational loads and scene complexity. A schematic diagram of this process and corresponding fusion time steps are shown on Fig. 5.

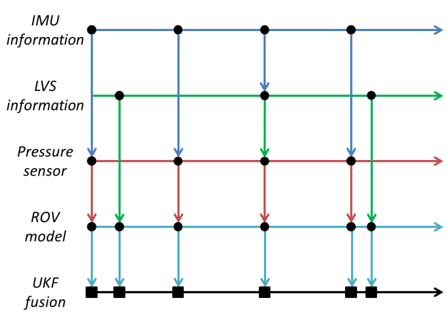

Fig. 5. Schematic diagram of the asynchronous sensor fusion approach.

The discrete model of the vehicle (1) is used as a system process model in which Δt is the time interval between the previous and the current time instance. The system process model is predicted forward in time and the mean and covariance of the state vector are updated only when a new measurement from either of the sensors is available. In the case, when only the IMU/Pressure sensor/LVS measurements/etc were received, the measurement model for the UKF algorithm is formulated in the form of the corresponding sensor model (for example, the IMU model (5), pressure sensor model (8), or the LVS model (13)). However, when the measurements from two or more sensors are available, the combination of the sensors models is used. For example, for the combination of the IMU + Pressure sensor + LVS, the threefold measurement model can be written as:

$$\mathbf{x} = \begin{bmatrix} h_{IMU}(\mathbf{x}) + \mathbf{w}_{IMU} \\ h_{PS}(\mathbf{x}) + \mathbf{w}_{PS} \\ h_{LVS}(\mathbf{x}) + \mathbf{w}_{LVS} \end{bmatrix} \tag{15}$$

Note that the sensor noise covariance matrix used in the UKF update step should be rewritten as well in accordance to the applied sensor model, for example, for the threefold combined sensor model as follows:

$$\mathbf{R} = \begin{bmatrix} \mathbf{R}_{IMU} & \mathbf{0}_{IMU\times PS} & \mathbf{0}_{IMU\times LVS} \\ \mathbf{0}_{PS\times IMU} & \mathbf{R}_{PS} & \mathbf{0}_{PS\times LVS} \\ \mathbf{0}_{LVS\times IMU} & \mathbf{0}_{LVS\times PS} & \mathbf{R}_{LVS} \end{bmatrix}. \tag{16}$$

V. Simulation Results

The developed localization algorithm was validated through various simulations under realistic levels of noises and disturbances.

The simulation scenario was to navigate the vehicle downwards along the aquaculture height with the constant vertical velocity $w = 0.1\,\mathrm{m/s}$. Simple controllers were applied in order to keep the vehicle along the predefined trajectory and the aquaculture in the field of view of the ROV. The STD of the gyro measurements was assumed as $0.05\,\mathrm{rad/s}$, the STD of the accelerometers was $0.03\,\mathrm{m/s}$, the STD of the pressure sensor was $0.1\,\mathrm{m}$, the STD of the LVS was $0.1\,\mathrm{m}$. The results of one simulation run for $50\,\mathrm{s}$ are shown on Fig. 6, where the trace of the covariance matrix is demonstrated as a measure of convergence of the filter.

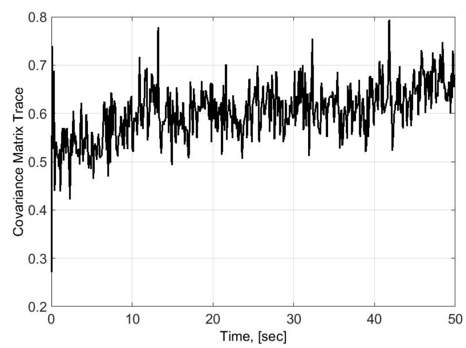

Fig. 6. Simulation results for one run: the trace of the state estimation covariance matrix.

A series of Monte-Carlo runs were conducted in order to evaluate the performance of the proposed sensor fusion algorithm for the position estimation only. Since we know a "true" state of the vehicle at each time instance, two metrics were used to examine the filter, namely, the root mean squared error (RMSE), to estimate the accuracy of the filter, and the normalized estimation error squared (NEES), to provide a measure of the filter consistency [20].

For each Monte-Carlo run j, $j = 1, \ldots, N_{runs}$ and each time step i, $i = 1, \ldots, N_{steps}$ we computed the NEES as:

$$NEES_i^j = \left(\mathbf{x}_i^j - \tilde{\mathbf{x}}_i^j\right)^T \left(\mathbf{P}_x^{ij}\right)^{-1} \left(\mathbf{x}_i^j - \tilde{\mathbf{x}}_i^j\right). \tag{17}$$

The average NEES (ANEES) over 10 Monte-Carlo runs and for each time step i is shown on Fig. 7(a) for $100\,\mathrm{s}$ simulation run and was computed as:

$$ANEES_i = \frac{1}{N_{runs}} \sum_{j=1}^{N_{runs}} NEES_i^j. \tag{18}$$

The average of the NEES over all Monte-Carlo runs and all times steps was 11.16. For a consistent filter, the ANEES

This is a DRAFT. As such it may not be cited in other works.
The citable Proceedings of the Conference will be published in
IEEE Xplore shortly after the conclusion of the conference.

tends towards the dimension of the state vector as the number of Monte-Carlo runs approaches infinity [20]. The comprehensive study of the filter performance in terms of ANEES and RMSE for different types of filters was conducted in [21]. According to this study, the performance of the asynchronous UKF applied in this work is close to the performance of the standard UKF.

The RMSE shown on Fig. 7(b) was computed for each time as well according to:

$$RMSE_i = \sqrt{\frac{1}{N_{runs}} \sum_{j=1}^{N_{runs}} \left(\mathbf{x}_i^j - \tilde{\mathbf{x}}_i^j\right)^T \left(\mathbf{x}_i^j - \tilde{\mathbf{x}}_i^j\right)}, \quad (19)$$

while the average RMSE over all steps for this case was $0.65\,\mathrm{m}$.

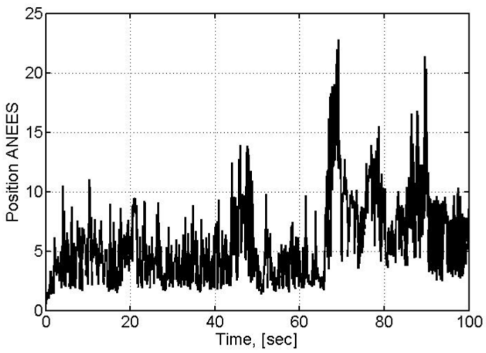

(a) The position ANEES averaged per time step

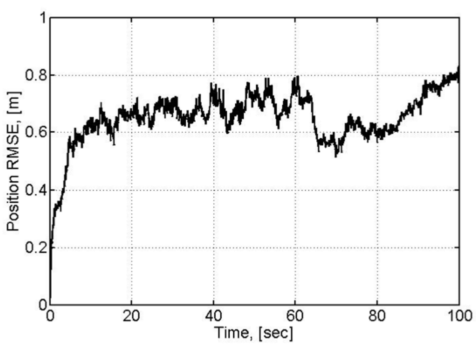

(b) The position RMSE averaged per time step.

Fig. 7. Simulation results for 10 Monte-Carlo runs.

VI. Conclusion and Future Work

This paper presented a state estimation algorithm for an autonomous underwater vehicle for aquaculture inspection. The algorithm can fuse the information from several sensors providing measurements with different and various frequencies. The performance of the algorithm was validated through simulations under real-world conditions and noises. As future work, we consider to conduct experiments and field tests to verify the proposed models and algorithms. Using other available sensors and information (for example, optical flow) in the state estimator along with applying observability constraints analysis to the filter is considered to be a part of future work as well.

References

[1] J. Guillen and A. Motova, "Summary of the 2013 Economic Performance Report on the EU Aquaculture Sector (STECF 13-30)," tech. rep., Scientific, Technical and Economic Committee for Fisheries (STECF), 2013.

[2] A. Fredheim, *Current Forces on Net Structures*. PhD thesis, Norwegian University of Science and Technology, 2005.

[3] P. Klebert, P. Lader, L. Gansel, and F. Oppedal, "Hydrodynamic Interactions on Net Panel and Aquaculture Fish Cages: A Review," *IEEE Journal of Ocean Engineering*, vol. 58, pp. 260–274, 2013.

[4] Y.-P. Zhao, T.-J. Xu, C.-W. Bi, G.-H. Dong, and S.-C. Liu, "The Numerical Simulation of Hydrodynamics of Fishing Net Cage," *Hydrodynamics - Theory and Model*, 2012.

[5] *An Autonomous Underwater Robotic Visual Inspection System for Cyprus' Offshore Aquaculture Industry (AQUABOT).* `http://aquaculturebot.com/`.

[6] S. Lynen, S. Omari, M. Wuest, M. Achtelik, and R. Siegwart, "Tightly Coupled Visual-Inertial Navigation System Using Optical Flow," in *2nd IFAC Workshop on Research, Education and Development of Unmanned Aerial Systems*, 2013.

[7] D. G. Kottas and S. I. Roumeliotis, "Efficient and Consistent Vision-Aided Inertial Navigation using Line Observation," in *IEEE International Conference on Robotics and Automation (ICRA)*, 2013.

[8] M. Bloesch, S. Omari, P. Fankhauser, H. Sommer, C. Gehring, J. Hwangbo, M. A.Hoepflinger, M. Hutter, and R. Y. Siegwart, "Fusion of Optical Flow and Inertial Measurements for Robust Egomotion Estimation," in *IEEE International Conference on Intelligent Robots and Systems (IROS)*, 2014.

[9] G. C. Karras, S. G. Loizou, and K. J. Kyriakopoulos, "Towards Semi-autonomous Operation of Under-actuated Underwater Vehicles: Sensor Fusion, On-line Identification and Visual Servo Control," *Autonomous Robots*, vol. 31, no. 1, pp. 67–86, 2011.

[10] T. I. Fossen, *Guidance and Control of Ocean Vehicles*. New York: Wiley, 1994.

[11] C. C. Constantinou, G. Georgiades, and S. G. Loizou, "A Laser Vision System for Relative 3-D Posture Estimation of an Underwater Vehicle to Mesh-like Targets," *under preparation*.

[12] S. Potyagaylo and S. G. Loizou, "Online Adaptive Geometry Predictor of Aquaculture Fish-Nets," in *Mediterranean Conference on Control and Automation (MED)*, June 2014.

[13] *Cyprus Coastal Ocean Forecasting and Observing System (CYCOFOS).* `http://www.oceanography.ucy.ac.cy/cycofos/`.

[14] *VideoRay Pro 4.* `http://videoray.com/homepage/professional-rovs/videoray-pro-4.html`.

[15] *InvenSence MPU-6050.* `http://www.invensense.com/mems/gyro/mpu6050.html`.

[16] L. Sciavicco and B. Siciliano, *Modelling and control of robot manipulators*. Springer Science & Business Media, 2012.

[17] C. C. Constantinou, G. Georgiades, S. Potyagaylo, and S. G. Loizou, "Modeling and Control for an Aquacutlure Inspection ROV," in *under preparation*.

[18] C. C. Constantinou, S. G. Loizou, G. Georgiades, S. Potyagaylo, and D. Skarlatos, "Adaptive Calibration of an Underwater Robot Vision System based on Hemispherical Optics," in *Autonomous Underwater Vehicles Conference (AUV)*, October 2014.

[19] A. D. Chambers, S. Scherer, L. Yoder, S. Jain, S. T. Nuske, and S. Singh, "Robust Multi-Sensor Fusion for Micro Aerial Vehicle Navigation in GPS-Degraded/Denied Environments," in *American Control Conference (ACC)*, June 2014.

[20] Y. Bar-Shalom, X. R. Li, and T. Kirubarajan, *Estimation with Applications to Tracking and Navigation*. New York: Wiley, 2001.

[21] G. P. Huang, A. I. Mourikis, and S. I. Roumeliotis, "A Quadratic-Compexity Observability-Constrained Uscented Kalman Filter for SLAM," *IEEE Transactions on Robotics*, vol. 29, no. 5, pp. 1226–1243, 2013.

978-0-933957-43-5 ©2015 MTS

This is a DRAFT. As such it may not be cited in other works.
The citable Proceedings of the Conference will be published in
IEEE Xplore shortly after the conclusion of the conference.